Development and assessment of the SMAP enhanced passive soil moisture product

S.K. Chan[a,*], R. Bindlish[b], P. O'Neill[b], T. Jackson[c], E. Njoku[a], S. Dunbar[a], J. Chaubell[a], J. Piepmeier[b], S. Yueh[a], D. Entekhabi[e], A. Colliander[a], F. Chen[d], M.H. Cosh[c], T. Caldwell[f], J. Walker[g], A. Berg[h], H. McNairn[i], M. Thibeault[j], J. Martínez-Fernández[k], F. Uldall[l], M. Seyfried[m], D. Bosch[n], P. Starks[o], C. Holifield Collins[p], J. Prueger[q], R. van der Velde[r], J. Asanuma[s], M. Palecki[t], E.E. Small[u], M. Zreda[v], J. Calvet[w], W.T. Crow[c], Y. Kerr[x]

[a] NASA Jet Propulsion Laboratory, California Institute of Technology, Pasadena, CA 91109, USA
[b] NASA Goddard Space Flight Center, Greenbelt, MD 20771, USA
[c] USDA ARS Hydrology and Remote Sensing Laboratory, Beltsville, MD 20705, USA
[d] Science Systems and Applications, Inc., Lanham, MD 20706, USA
[e] Massachusetts Institute of Technology, Cambridge, MA 02139, USA
[f] University of Texas, Austin, TX 78713, USA
[g] Monash University, Clayton, Vic 3800, Australia
[h] University of Guelph, Guelph, ON N1G 2W1, Canada
[i] Agriculture and Agri-Food Canada, Ottawa, ON, K1A OC6, Canada
[j] Comisión Nacional de Actividades Espaciales (CONAE), Buenos Aires, Argentina
[k] Instituto Hispano Luso de Investigaciones Agrarias (CIALE), Universidad de Salamanca, 37185 Salamanca, Spain
[l] Center for Hydrology, Technical University of Denmark, Copenhagen, Denmark
[m] USDA ARS Northwest Watershed Research Center, Boise, ID 83712, USA
[n] USDA ARS Southeast Watershed Research Center, Tifton, GA 31793, USA
[o] USDA ARS Grazinglands Research Laboratory, El Reno, OK 73036, USA
[p] USDA ARS Southwest Watershed Research Center, Tucson, AZ 85719, USA
[q] USDA ARS National Laboratory for Agriculture and the Environment, Ames, IA 50011, USA
[r] University of Twente, Enschede, Netherlands
[s] University of Tsukuba, Tsukuba, Japan
[t] NOAA National Climatic Data Center, Asheville, NC 28801, USA
[u] University of Colorado, Boulder, CO 80309, USA
[v] University of Arizona, Tucson, AZ 85751, USA
[w] CNRM-GAME, UMR 3589 (Météo-France, CNRS), Toulouse, France
[x] CESBIO-CNES, Toulouse, France

ARTICLE INFO

ABSTRACT

Launched in January 2015, the National Aeronautics and Space Administration (NASA) Soil Moisture Active Passive (SMAP) observatory was designed to provide frequent global mapping of high-resolution soil moisture and freeze-thaw state every two to three days using a radar and a radiometer operating at L-band frequencies. Despite a hardware mishap that rendered the radar inoperable shortly after launch, the radiometer continues to operate nominally, returning more than two years of science data that have helped to improve existing hydrological applications and foster new ones.

Beginning in late 2016 the SMAP project launched a suite of new data products with the objective of recovering some high-resolution observation capability loss resulting from the radar malfunction. Among these new data products are the SMAP Enhanced Passive Soil Moisture Product that was released in December 2016, followed by the SMAP/Sentinel-1 Active-Passive Soil Moisture Product in April 2017.

This article covers the development and assessment of the SMAP Level 2 Enhanced Passive Soil Moisture Product (L2_SM_P_E). The product distinguishes itself from the current SMAP Level 2 Passive Soil Moisture Product (L2_SM_P) in that the soil moisture retrieval is posted on a 9 km grid instead of a 36 km grid. This is made possible by first applying the Backus-Gilbert optimal interpolation technique to the antenna temperature (T_A) data in the original SMAP Level 1B Brightness Temperature Product to take advantage of the overlapped

radiometer footprints on orbit. The resulting interpolated T_A data then go through various correction/calibration procedures to become the SMAP Level 1C Enhanced Brightness Temperature Product (L1C_TB_E). The L1C_TB_E product, posted on a 9 km grid, is then used as the primary input to the current operational SMAP baseline soil moisture retrieval algorithm to produce L2_SM_P_E as the final output. Images of the new product reveal enhanced visual features that are not apparent in the standard product. Based on *in situ* data from core validation sites and sparse networks representing different seasons and biomes all over the world, comparisons between L2_SM_P_E and *in situ* data were performed for the duration of April 1, 2015–October 30, 2016. It was found that the performance of the enhanced 9 km L2_SM_P_E is equivalent to that of the standard 36 km L2_SM_P, attaining a retrieval uncertainty below 0.040 m^3/m^3 unbiased root-mean-square error (ubRMSE) and a correlation coefficient above 0.800. This assessment also affirmed that the Single Channel Algorithm using the V-polarized T_B channel (SCA-V) delivered the best retrieval performance among the various algorithms implemented for L2_SM_P_E, a result similar to a previous assessment for L2_SM_P.

1. Introduction

The synergy of active (radar) and passive (radiometer) technologies at L-band microwave frequencies in the National Aeronautics and Space Administration (NASA) Soil Moisture Active Passive (SMAP) mission provides a unique remote sensing opportunity to measure soil moisture with unprecedented accuracy, resolution, and coverage (Entekhabi et al., 2014). Driven by the needs in hydroclimatological and hydrometeorological applications, the SMAP observatory was designed to meet a soil moisture retrieval accuracy requirement of 0.040 m^3/m^3 unbiased root-mean-square error (ubRMSE) or better at a spatial resolution of 10 km over non-frozen land surfaces that are free of excessive snow, ice, and dense vegetation coverage (Entekhabi et al., 2014).

In July 2015, SMAP's radar stopped working due to an irrecoverable hardware failure, leaving the radiometer as the only operational instrument onboard the observatory. Since the beginning of science data acquisition in April 2015, the radiometer has been collecting L-band (1.41 GHz) brightness temperature (T_B) data at a spatial resolution of 36 km, providing global coverage every two to three days. The relatively high fidelity of the data provided by the radiometer's radio-frequency-interference (RFI) mitigation hardware (Piepmeier et al., 2015b; Mohammed, et al., 2016), along with the observatory's full 360-degree view that offers both fore- and aft-looking observations, presents unique advantages for SMAP data to advance established hydrological applications (Koster et al., 2016) and foster new ones (Yueh et al., 2016).

Despite the loss of the radar, SMAP is committed to providing high-resolution observations to the extent that is possible. This initiative of acquiring high-resolution information proceeds in two distinct approaches. The first approach involves combining the current SMAP coarse-resolution passive observations with high-resolution radar observations from *other* satellites in space to produce an operational soil moisture product similar to the now discontinued SMAP Level 2 Active-Passive Soil Moisture Product (L2_SM_AP). To attain this objective, the high-resolution synthetic aperture radar (SAR) data from the European Space Agency (ESA) Sentinel-1 C-band radar constellation (Torres et al., 2012) represent the most optimal candidate data source that would provide partial fulfillment of the original science benefits of L2_SM_AP. Although there are technical challenges due to data latency, global coverage, revisit frequency, and retrieval performance from such a combined L/C-band SMAP/Sentinel-1 soil moisture product, these challenges are expected to be mitigated over time under the close collaboration between the two mission teams. The resulting SMAP/Sentinel-1 Level 2 Active-Passive Product (L2_SM_SP) will be available to the public in April 2017.

The second approach is based on the application of the Backus-Gilbert (BG) optimal interpolation technique (Poe, 1990; Stogryn, 1978) to the antenna temperature (T_A) measurements in the original SMAP Level 1B Brightness Temperature Product (L1B_TB) (Piepmeier et al., 2015a, 2015b). The resulting interpolated T_A data then go

through the standard correction/calibration procedures to produce the SMAP Level 1C Enhanced Brightness Temperature Product (L1C_TB_E) on a set of 9 km grids (Chaubell et al., 2016). The objective of the BG interpolation as implemented by SMAP is to achieve optimal brightness temperature (T_B) estimates at arbitrary locations as if original observations were available at the same locations (Poe, 1990). This estimation is achieved by linearly combining optimally weighted radiometric measurements overlapped in both along- and across-scan directions. The BG procedure is an improvement over what the current SMAP Level 1C Brightness Temperature Product (L1C_TB) (Chan et al., 2014, 2015) offers, in that it makes explicit use of antenna pattern information and finer grid posting to more fully capture the high spatial frequency information in the original oversampled radiometer measurements in the along-scan direction (Chaubell, 2016). It is important to note that this recovery of high spatial frequency information as implemented in this approach primarily comes from interpolation instead of beam sharpening. As such, the native resolution of the interpolated data remains to be about the same as the spatial extent projected on earth surface by the 3-dB beamwidth of the radiometer. For SMAP, this spatial extent is roughly an ellipse with 36 km as its minor axis and 47 km as its major axis (Entekhabi et al., 2014). As the SMAP project adopted the square root of footprint *area* as the definition of native resolution of the radiometer, the corresponding native resolution is estimated to be $(\pi / 4 \times 36 \times 47)^{1/2} \sim 36$ km. The resulting L1C_TB_E data are posted on the EASE Grid 2.0 projection (Brodzik et al., 2012, 2014) at a grid spacing of 9 km, even though the data actually exhibit a native resolution of ~36 km. The L1C_TB_E product is then used as the primary input in subsequent passive geophysical inversion to produce the SMAP Level 2 Enhanced Passive Soil Moisture Product (L2_SM_P_E) (O'Neill et al., 2016), which is the focus of this paper.

The retrieval performance of L2_SM_P_E was assessed and reported in this paper using > 1.5 years (April 1, 2015–October 30, 2016) of *in situ* data from core validation sites (CVSs) and sparse networks representing different seasons and biomes all over the world. The assessment findings presented in this paper represent a significant extension of the work reported in (Chan et al., 2016). Additional metric statistics from this assessment can be found in a separate report that covers the standard and enhanced passive soil moisture products (Jackson et al., 2016).

2. Product development

The SMAP observatory was to present a unique opportunity to demonstrate the synergy of radar and radiometer observations at L-band frequencies in the remote sensing of soil moisture and freeze/thaw state detection from space. Unfortunately, this demonstration was shortened due to a hardware failure that eventually halted the operation of the radar after about three months of operation. While the loss necessarily ended the operational production of several key soil moisture and freeze/thaw data products that rely on the high-resolution radar data, it also spurred the development of several new data products designed to

recover as much high-resolution information as possible.

Table 1 shows a list of SMAP data products that are or will be in routine operational production. There are two main groups of data products in the table: enhanced products (with asterisks) and standard products (without asterisks). The standard products are those that have been available since the beginning of the mission and will continue to be available operationally. The enhanced products, on the other hand, represent new products developed after the loss of the SMAP radar; these products contain enhanced information derived from the existing radiometer observations or new external data from other satellites. For example, the L2_SM_SP product is a product derived from the SMAP's L-band radiometer observations and the Sentinel-1's C-band SAR data (Torres et al., 2012). This product will be available to the public in April 2017. Other enhanced products (L1C_TB_E L2_SM_P_E, L3_SM_P_E, L3_FT_P, and L3_FT_P_E) are derived primarily from the existing radiometer observations. These products have been available to the public since December 2016. Of these radiometer-only enhanced products, L1C_TB_E and L2_SM_P_E will be covered in greater detail in Sections 2.1 and 2.2, respectively. A more comprehensive list of SMAP data products, including those that have been discontinued, can be found in Entekhabi et al. (2014).

2.1. Enhanced brightness temperature

Passive soil moisture inversion begins with T_B observations. For SMAP, to more fully capture the information in the oversampled along-scan T_B observations, the BG interpolation technique is applied to the T_A measurements in the standard L1B_TB product in the SMAP's Science Data System (SDS). The resulting interpolated T_A data then go through the standard correction/calibration procedures to produce the L1C_TB_E product. The BG implementation in SDS follows the same approach described in (Poe, 1990) that makes use of antenna pattern information to produce T_B estimates at arbitrary sampling locations. The procedure is considered optimal in the sense that its estimates are supposed to minimize differences relative to what would have been measured had the instrument actually sampled at the same locations. For immediate application to soil moisture and freeze/thaw state detection in SMAP product production, the T_B values in L1C_TB_E are posted on the 9 km EASE Grid 2.0 in global cylindrical projection, north polar projection, and south polar projection. Only the T_B values on global projection are used in passive soil moisture inversion. A more in-depth account of the theory behind the BG implementation in SDS can be found in the Algorithm Theoretical Basis Document (ATBD) (Chaubell, 2016) and Assessment Report (Piepmeier et al., 2016) that accompany the product. Besides the ATBD, the Product Specification Document (PSD) (Chan and Dunbar, 2016) is also available on the NASA Distributed Active Archive Center (DAAC) at the National Snow and Ice Data Center (NSIDC) for informed applications of the product.

Fig. 1 illustrates the horizontally polarized T_B observations obtained by SMAP between December 15–17, 2016 over the Amazon basin before and after the application of BG interpolation. This area was selected because the domain features well-defined river tracks punctuated with highly visible fine-scale spatial structures in the midst of a relatively homogeneous background. It is clear from the comparison that the enhanced L1C_TB_E (Fig. 1a) is able to reveal spatial features that are concealed or not immediately obvious in the standard L1C_TB (Fig. 1b). Overall, the L1C_TB_E image also presents a less pixelated representation of the original T_B data due to its posting on a finer grid.

It is important to note that the improvement in L1C_TB_E image quality primarily comes from an interpolation scheme that is an improvement over what is used in the standard product. The interpolation in L1C_TB_E more fully captures the information from the oversampled along-scan T_B observations without degrading the native resolution of the radiometer. This aspect regarding the native resolution of the product had been extensively vetted during product development in a series of matchup analyses using the original time-ordered L1B_TB T_B

data points as the benchmark data set. The matchup analyses began with collocating pairs of L1C_TB_E T_B data points and L1B_TB T_B data points that are within a small distance from each other (< 2 km, which is less than the L1B_TB geolocation error allocation (Piepmeier et al., 2015b)). The collocated pairs were stored separately for ascending and descending passes, and also for fore- and aft-looking observations to minimize azimuthal mismatch. The collocated data pairs from these four matchup collections (*i.e.*, ascending/fore, ascending/aft, descending/fore, and descending/aft) were then averaged over all orbits between April 1, 2015 and October 30, 2016 for all grid cells in the 9 km global EASE Grid 2.0 projection. Even though the L1C_TB_E data values are posted on a grid, they are expected to be almost identical to the corresponding L1B_TB data values at the same grid locations due to the close proximity between the two.

Given their impulse-like radiometric responses, small and isolated islands in the ocean provide ideal locations to compare the native resolution of L1C_TB_E against the known native resolution of L1B_TB using the collocated data pairs described above. This approach of using discrete islands to evaluate data native resolution has been extensively explored in the study of resolution-enhanced scatterometer data (Bradley and Long, 2014). Fig. 2 describes one such comparison performed over Ascension Island (7.93°S,14.417°W) located approximately midway between the coasts of Brazil and Africa in the South Atlantic Ocean. The island is about 10.07 km across and exhibits near azimuthal symmetry. Based on the peak values of L1C_TB_E (Fig. 2a) and L1B_TB (Fig. 2b), contours that correspond to one half of their respective peak values were estimated around the island. These 3-dB contours, which are indicative of the native resolution of the underlying data, are depicted by the blue lines in the figures. The magenta lines in both figures are identical; they correspond to the 3-dB contours estimated based on the geometry of the projected instantaneous field-of-view (IFOV) of the radiometer. The good agreement in 3-dB contour estimation between radiometric estimation (blue lines) and geometric calculation (magenta lines) confirms that small and isolated islands such as Ascension Island can indeed provide a good approximation for the impulse response from a point target.

The comparison shows that after BG interpolation the 3-dB contour of L1C_TB_E in Fig. 2a is about the same size as the 3-dB contour of L1B_TB in Fig. 2b, confirming that the enhanced product preserves the native resolution and noise characteristics of the radiometer while providing an optimal interpolation approach that more fully utilizes the oversampled along-scan T_B measurements in the original data. Further

Table 1
SMAP data products that are or will be in routine operational production.

| Product	Description	Grid resolution	Latency
L1A_Radiometer	Radiometer telemetry in time order	N\A	12 h
L1B_TB	Radiometer time-ordered T_B	N\A	12 h
L1C_TB	Radiometer gridded T_B	36 km	12 h
L1C_TB_E*	Radiometer gridded T_B (enhanced)	9 km	12 h
L2_SM_P	Soil moisture (radiometer)	36 km	24 h
L2_SM_P_E*	Soil moisture (radiometer, enhanced)	9 km	24 h
L2_SM_SP*	Soil moisture (radiometer + Sentinel-1 radar)	3 km	Best effort
L3_FT_P*	Freeze/thaw state (radiometer)	36 km	50 h
L3_FT_P_E*	Freeze/thaw state (radiometer, enhanced)	9 km	50 h
L3_SM_P	Soil moisture (radiometer)	36 km	50 h
L3_SM_P_E*	Soil moisture (radiometer, enhanced)	9 km	50 h
L4_SM	Soil moisture (surface and root zone)	9 km	7 days
L4_C	Carbon net ecosystem exchange (NEE)	9 km	14 days
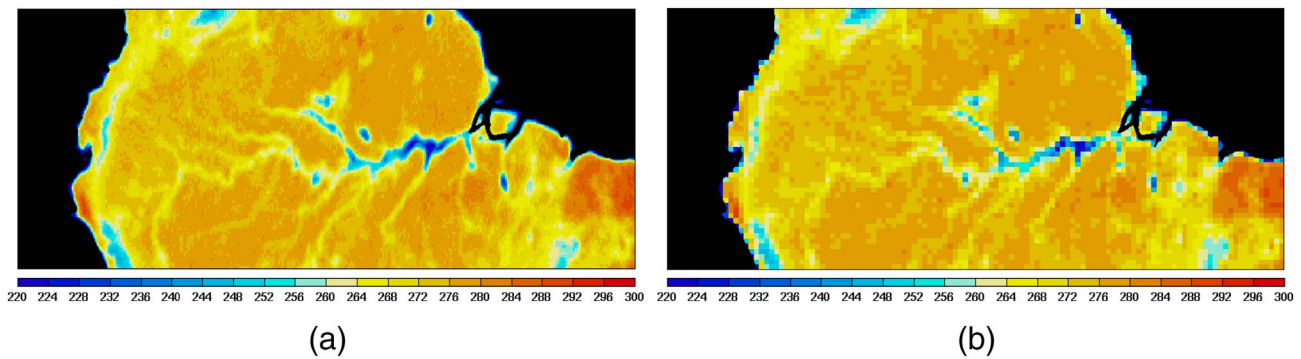
Fig. 1. SMAP horizontally polarized T$_B$ observations obtained between December 15–17, 2016 over the Amazon basin: (a) L1C_TB_E and (b) L1C_TB.
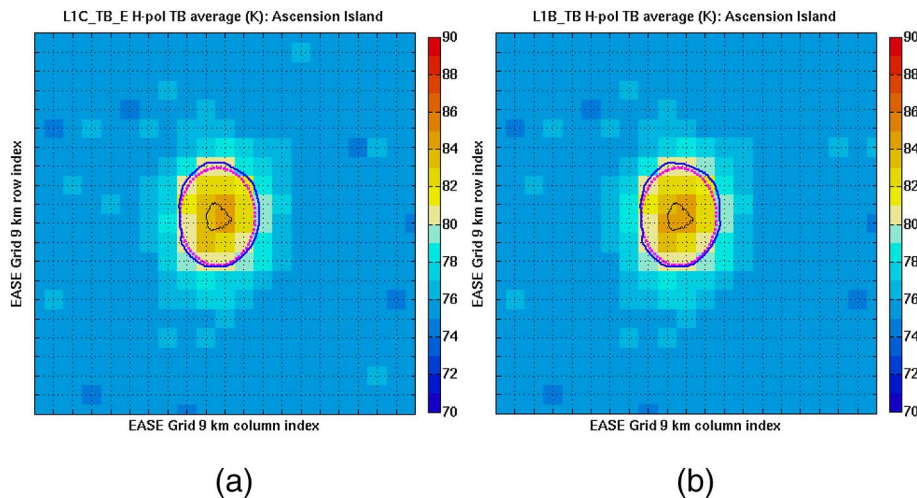

Fig. 2. Comparison of data native resolution between L1C_TB_E and L1B_TB based on radiometric estimation (blue lines) and geometric calculation (magenta lines): (a) L1C_TB_E and (b) L1B_TB. (For interpretation of the references to colour in this figure legend, the reader is referred to the web version of this article.)

Table 2
Ancillary data used in L2_SM_P_E and L2_SM_P processing.

Ancillary data	Grid resolution	Time resolution	Primary data source
Water fraction	3 km	Static	MODIS MOD44W (Chan et al., 2013)
Urban fraction	3 km	Static	Global Rural Urban Mapping Project (GRUMP) (Das, 2013a, 2013b)
DEM slope variability	3 km	Static	USGS GMTED 2010 (Podest and Crow, 2013)
Soil texture	3 km	Static	FAO Harmonized World Soil Database (HWSD) (Das, 2013a, 2013b)
Land cover	3 km	Static	MODIS MCD12Q1 (V051) (Kim, 2013)
NDVI	3 km	2000–2013	MODIS MOD13A2 (V005) (Chan, 2013)
Snow fraction	9 km	Daily	NOAA IMS (Kim and Molotch, 2011)
Freeze/thaw fraction	9 km	1 hourly	GMAO GEOS-5 (SMAP, 2015)
Soil temperatures	9 km	1 hourly	GMAO GEOS-5 (SMAP, 2015)
Precipitation	9 km	3 hourly	GMAO GEOS-5 (Dunbar, 2013)

analyses on other small and isolated islands yielded the same conclusions. The T$_B$ signatures between L1C_TB_E in Fig. 2a and L1B_TB in Fig. 2b are similar, suggesting that the current BG implementation indeed preserves the original data at locations where L1B_TB measurements are available.

The native resolution of L1C_TB_E determines the spatial scale by which the subsequent L2_SM_P_E should be developed and assessed. It was found that when 3 km ancillary data (Table 2) are aggregated as inputs to L2_SM_P_E that is posted on a 9 km grid, a contributing domain of 33 km × 33 km (Section 3.1) is necessary to cover a spatial extent similar to the native resolution of the radiometer, as shown in Fig. 3. This contributing domain was thus adopted in L2_SM_P_E product development (Section 2.2) and assessment (Section 3).

It is anticipated that future SDS BG implementations could improve the current L1C_TB_E native resolution beyond the radiometer IFOV. Such an improvement will require an alternate contributing domain that approximates the new native resolution in revised L2_SM_P_E

development and assessment.

2.2. Enhanced passive soil moisture

The development of L2_SM_P_E follows a close parallel with that of L2_SM_P (Chan et al., 2016; O'Neill et al., 2015). Both products share the same basic implementation elements, ranging from processing flow, ancillary data, and retrieval algorithms. Fig. 4 illustrates the flow of the L2_SM_P_E processor. The fore- and aft-look T$_B$ observations in L1C_TB_E are first combined to provide the primary input to the processor. Static and dynamic ancillary data (Table 2) preprocessed on finer grid resolutions are then brought into the processing to evaluate the feasibility of the retrieval. If retrieval is deemed feasible at a given location, the processor will further evaluate the quality of the retrieval. When surface conditions favorable to soil moisture retrieval are identified, corrections for surface roughness, effective soil temperature, vegetation water content, and radiometric contribution by water bodies
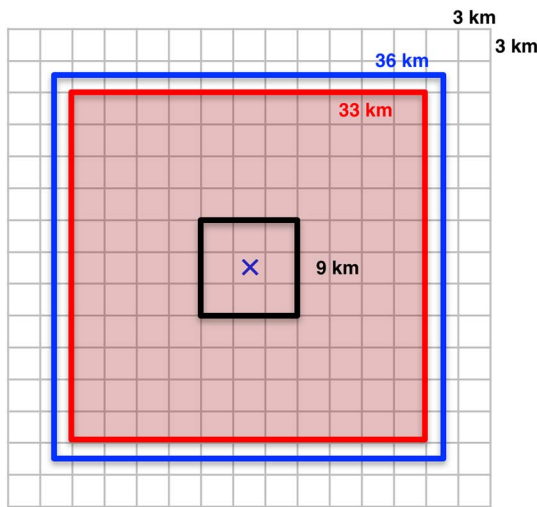
Fig. 3. With L2_SM_P_E (black) and ancillary data (gray) posted at 9 km and 3 km, respectively, a contributing domain of 33 km × 33 km (red) is necessary to cover a spatial extent similar to the native resolution (blue) of the radiometer. (For interpretation of the references to colour in this figure legend, the reader is referred to the web version of this article.)

are applied. The baseline soil moisture retrieval algorithm is then invoked with T$_B$ observations and ancillary data as inputs to produce L2_SM_P_E on the same 9 km EASE Grid 2.0 global projection as the input L1C_TB_E. A full description of L2_SM_P_E data contents can be found in the Product Specification Document (Chan, 2016).

Because of its improved representation of the original T$_B$ data, the enhanced 9 km L1C_TB_E product contains additional spatial information that is not available in the standard 36 km L1C_TB product, as exemplified in a series of spectral analysis on small and isolated islands

in the ocean (Piepmeier et al., 2016). When used as the primary input to the enhanced 9 km L2_SM_P_E product, the additional spatial information results in enhanced visual details that are also not available in the standard 36 km L2_SM_P product. Fig. 5 contrasts the amount of visual details between L2_SM_P_E (Fig. 5a) and L2_SM_P (Fig. 5b) over the vegetation transition region in Africa. After the application of the baseline soil moisture retrieval algorithm to L1C_TB_E, the resulting L2_SM_P_E on a 9 km grid shows a higher acuity compared with L2_SM_P on a 36 km grid. This enhancement in spatial details is further illustrated in Fig. 5c in which the soil moisture variability of L2_SM_P_E (black line) and L2_SM_P (red line) along the two identical magenta lines in Fig. 5a and b is plotted together. The enhanced and standard products mostly track each other and follow the same macroscopic spatial patterns along the transect without obvious bias or unusual artifacts. In addition, there are locations (*e.g.* between column indices 512 and 515 in Fig. 5c) where L2_SM_P_E appears to capture fine-scale soil moisture variability that is not available in L2_SM_P. It is important to note that throughout the L2_SM_P_E processing, no new or additional ancillary datasets other than those listed in Table 2 are brought into the processing. The observed enhanced spatial details revealed in L2_SM_P_E are thus primarily contributed by the additional spatial information in L1C_TB_E.

On a global scale, the enhanced product exhibits the expected geographical patterns of soil moisture. Fig. 6 represents a three-day composite of 6:00 am descending L2_SM_P_E between September 20–22, 2016. The expected patterns of L2_SM_P_E soil moisture estimates in m^3/m^3 qualitatively affirm the soundness of the underlying baseline soil moisture retrieval algorithm. Section 3 covers the quantitative aspect of the assessment for the product based on comparison with *in situ* soil moisture observations.
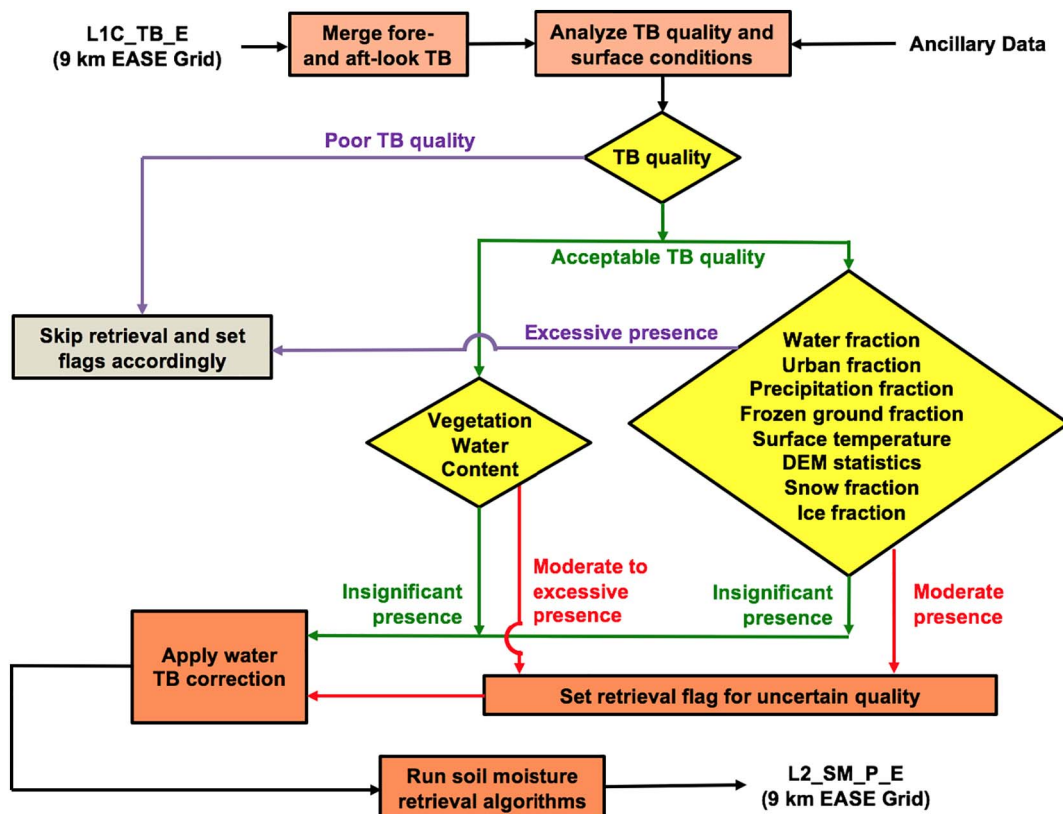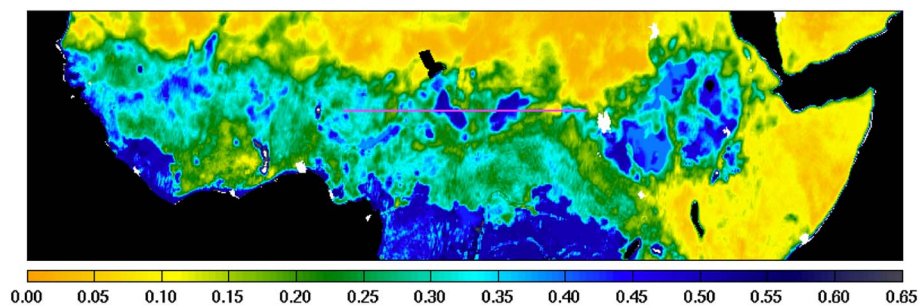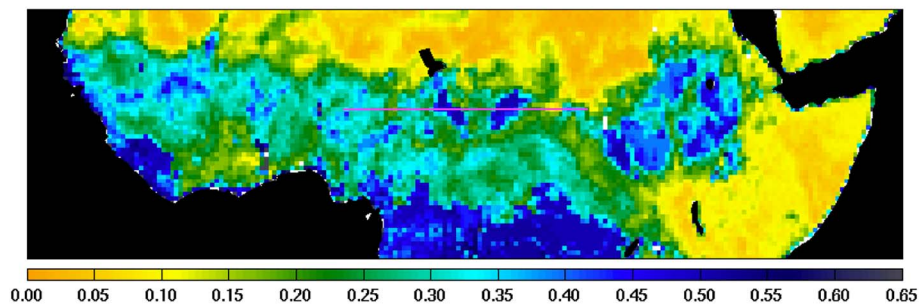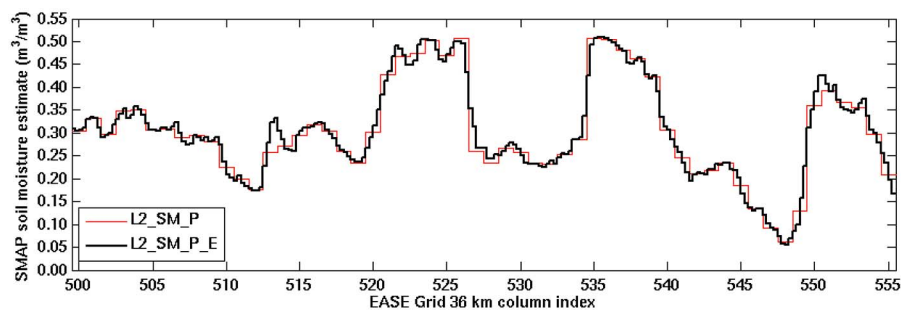

Fig. 4. L2_SM_P_E processor design. The processor uses L1C_TB_E and ancillary data as primary inputs to perform geophysical inversion under favorable surface conditions. The resulting L2_SM_P_E soil moisture estimates are posted on the same 9 km EASE Grid 2.0 global projection as the input L1C_TB_E.

Fig. 5. Soil moisture estimates in m^3/m^3 of (a) L2_SM_P_E, (b) L2_SM_P, and (c) L2_SM_P_E and L2_SM_P along the two identical magenta lines in (a) and (b). (For interpretation of the references to colour in this figure legend, the reader is referred to the web version of this article.)

(a)

(b)

(c)
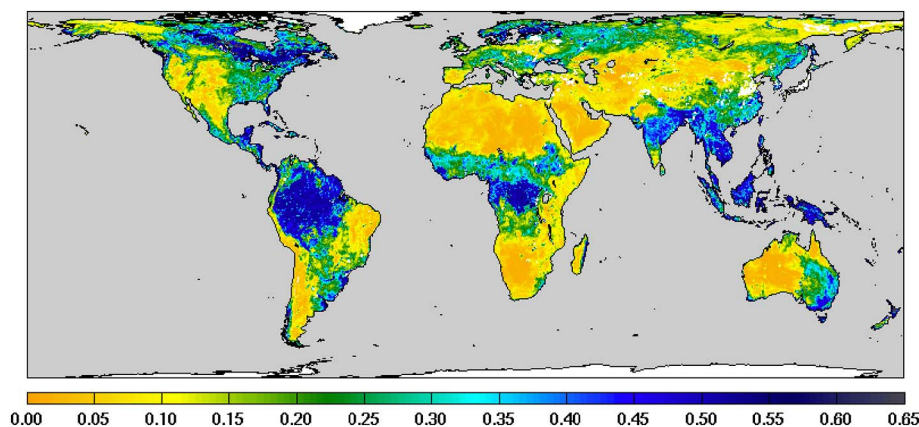
Fig. 6. Global pattern of soil moisture estimates in m^3/m^3 of L2_SM_P_E based on 6:00 am descending T$_B$ data between September 20–22, 2016.

3. Product assessment

The retrieval accuracy of L2_SM_P_E was assessed using the same validation methodologies for L2_SM_P as reported in (Chan et al., 2016; Colliander et al., 2017). Nineteen months (April 2015 through October 2016) of *in situ* soil moisture observations were used as ground truth to evaluate the performance of the product. Much deliberation had been

made before the SMAP launch in the selection of these *in situ* data sources based on criteria that would ensure data quality, sensor maintenance and calibration stability, biome diversity, and geographical representativeness. The *in situ* data consist of scaled aggregations of *in situ* soil moisture observations at a nominal soil depth of 5 cm to mimic L2_SM_P_E soil moisture estimates at satellite footprint scale. All *in situ* data were provided through a collaboration with domestic and

Table 3
CVSs used in L2_SM_P_E assessment.

CVS (latitude, longitude)	Location	Climate regime	Land cover type
Walnut Gulch (31.75°, −110.03°)	Arizona, USA	Arid	Shrub open
Reynolds Creek (43.19°, −116.75°)	Idaho, USA	Arid	Grasslands
TxSON (30.35°, −98.73°)	Texas, USA	Temperate	Grasslands
Fort Cobb (35.38°, −98.64°)	Oklahoma, USA	Temperate	Grasslands/croplands
Little Washita (34.86°, −98.08°)	Oklahoma, USA	Temperate	Grasslands
South Fork (42.42°, −93.41°)	Iowa, USA	Cold	Croplands
Little River (31.67°, −83.60°)	Georgia, USA	Temperate	Cropland/natural mosaic
Kenaston (51.47°, −106.48°)	Canada	Cold	Croplands
Carman (49.60°, −97.98°)	Canada	Cold	Croplands
Monte Buey (−32.91°, −62.51°)	Argentina	Arid	Croplands
REMEDHUS (41.29°, −5.46°)	Spain	Temperate	Croplands
Twente (52.26°, 6.77°)	Netherlands	Temperate	Cropland/natural mosaic
HOBE (55.97°, 9.10°)	Denmark	Temperate	Croplands
Mongolia (46.05°, 106.76°)	Mongolia	Cold	Grasslands
Yanco (−34.86°, 146.16°)	Australia	Arid	Croplands

international calibration/validation (cal/val) partners who operate and maintain calibrated soil moisture measuring sensors in their core validation sites (CVSs) (Colliander et al., 2017; Smith et al., 2012; Yee et al., 2016) or sparse networks (Chen et al., 2017).

Agreement between the L2_SM_P_E soil moisture estimates and *in situ* data over space and time are reported in four metrics: 1) unbiased root-mean-square error (ubRMSE), 2) bias (defined as L2_SM_P_E minus *in situ* data), 3) root-mean-square error (RMSE), and 4) correlation (R).

Together, these metrics provide a more complete description of product performance than any one alone (Entekhabi et al., 2010). Among these metrics, however, the ubRMSE computed from *in situ* data comparison at CVSs is adopted for reporting the product accuracy of L2_SM_P_E, with an accuracy target of 0.040 m³/m³ that mimics the SMAP Level 1 mission accuracy requirement for the now discontinued SMAP Level 2 Active-Passive Soil Moisture Product (L2_SM_AP) (Entekhabi et al., 2010).

In addition to L2_SM_P_E, the retrieval performance of L2_SM_P and soil moisture estimates by the Soil Moisture and Ocean Salinity (SMOS) mission (Kerr et al., 2016) was also provided for comparison. In this assessment, both L2_SM_P_E and L2_SM_P were based on version R13080 of the standard L1B_TB product, whereas versions 551 and 621 of the SMOS Level 2 soil moisture product were used for April 1–May 4, 2015 and May 5, 2015–October 31, 2016, respectively. For both SMAP and SMOS soil moisture data products, only those soil moisture estimates whose retrieval quality fields indicated good retrieval quality were considered and used in metric calculations. The selection involved data of recommended quality as indicated in the retrieval quality flag for the SMAP product, and data with unset FL_NO_PROD and retrieval DQX < 0.07 for the SMOS product.

Compared with L2_SM_P, L2_SM_P_E is expected to exhibit a higher serial correlation of retrieval uncertainty over space. This higher correlation is a direct result of the original L1B_TB interpolated on a finer grid posting (9 km) for L2_SM_P_E than the original grid posting (36 km) for L2_SM_P. A full investigation into the spatial correlation characteristics between the standard and enhanced products is beyond the scope of this assessment.

3.1. Core validation sites

Although in general limited in quantity and spatial extent, CVSs provide *in situ* soil moisture observations that, when properly scaled and aggregated, provide a representative spatial average of soil moisture at the spatial scale of L2_SM_P_E (Section 2.1). In this assessment, CVS *in situ* data between April 2015 and October 2016 from a total of 15 global sites were aggregated over a contributing domain of 33 km × 33 km (Fig. 3 in Section 2.1) around the sites. This area was chosen so that on a 9 km grid the resulting aggregated ancillary data

Table 4
Comparison between the 6:00 am descending L2_SM_P_E soil moisture estimates and CVS *in situ* soil moisture observations between April 2015 and October 2016.

CVS	ubRMSE (m³/m³)			Bias (m³/m³)			RMSE (m³/m³)			Correlation (R)			N		
	SCA-H	SCA-V	DCA	SCA-H	SCA-V	DCA	SCA-H	SCA-V	DCA	SCA-H	SCA-V	DCA	SCA-H	SCA-V	DCA
Reynolds Creek	0.039	0.040	0.057	−0.059	−0.023	0.007	0.071	0.046	0.058	0.572	0.598	0.558	86	97	96
Walnut Gulch	0.021	0.024	0.038	−0.011	0.011	0.035	0.024	0.026	0.052	0.759	0.813	0.800	93	118	115
TxSON	0.031	0.032	0.041	−0.064	−0.015	0.056	0.071	0.036	0.069	0.935	0.921	0.827	153	153	152
Fort Cobb	0.032	0.028	0.045	−0.086	−0.056	−0.017	0.091	0.062	0.048	0.858	0.883	0.817	244	247	247
Little Washita	0.023	0.022	0.042	−0.062	−0.027	0.026	0.066	0.035	0.050	0.911	0.920	0.837	246	246	245
South Fork	0.062	0.054	0.054	−0.071	−0.062	−0.050	0.094	0.082	0.074	0.597	0.646	0.637	159	162	162
Little River	0.034	0.028	0.041	0.048	0.087	0.144	0.059	0.092	0.150	0.871	0.887	0.755	229	229	229
Kenaston	0.034	0.022	0.040	−0.064	−0.040	−0.001	0.072	0.046	0.040	0.808	0.854	0.515	145	145	145
Carman	0.094	0.056	0.053	−0.087	−0.088	−0.077	0.128	0.104	0.093	0.463	0.611	0.535	157	158	158
Monte Buey	0.075	0.051	0.042	−0.022	−0.020	−0.025	0.078	0.055	0.049	0.754	0.840	0.724	126	135	137
REMEDHUS	0.037	0.042	0.054	−0.024	−0.007	0.010	0.044	0.042	0.055	0.897	0.872	0.837	197	196	189
Twente	0.072	0.056	0.056	0.003	0.013	0.028	0.072	0.057	0.063	0.888	0.885	0.784	238	242	241
HOBE	0.048	0.036	0.063	0.004	−0.009	−0.012	0.048	0.037	0.064	0.700	0.863	0.789	104	104	104
Mongolia	0.032	0.036	0.036	−0.009	−0.006	−0.006	0.033	0.037	0.037	0.736	0.728	0.730	139	102	116
Yanco	0.051	0.043	0.045	0.000	0.020	0.035	0.051	0.048	0.057	0.960	0.964	0.943	170	172	170
L2_SM_P_E over a 33 km × 33 km contributing domain	0.046	0.038	0.047	−0.034	−0.015	0.010	0.067	0.054	0.064	0.781	0.819	0.739			
L2 SMOS averaged over a 33 km × 33 km contributing domain	0.051			−0.023			0.071			0.698					
L2_SM_P over a 36 km × 36 km contributing domain	0.044	0.037	0.043	−0.033	−0.014	0.010	0.065	0.052	0.063	0.796	0.822	0.738			
L2 SMOS averaged over a 36 km × 36 km contributing domain	0.051			−0.024			0.072			0.713					

Table 5

Comparison between the 6:00 pm ascending L2_SM_P_E soil moisture estimates and CVS *in situ* soil moisture observations between April 2015 and October 2016.

CVS	ubRMSE (m³/m³)			Bias (m³/m³)			RMSE (m³/m³)			Correlation (R)			N		
	SCA-H	SCA-V	DCA	SCA-H	SCA-V	DCA	SCA-H	SCA-V	DCA	SCA-H	SCA-V	DCA	SCA-H	SCA-V	DCA
Reynolds Creek	0.046	0.042	0.060	− 0.075	− 0.042	− 0.005	0.088	0.059	0.060	0.452	0.651	0.630	79	106	96
Walnut Gulch	0.027	0.029	0.042	− 0.031	− 0.019	− 0.000	0.041	0.034	0.042	0.622	0.676	0.631	102	165	141
TxSON	0.028	0.028	0.033	− 0.058	− 0.018	0.031	0.065	0.034	0.045	0.930	0.929	0.893	178	178	178
Fort Cobb	0.039	0.035	0.046	− 0.087	− 0.069	− 0.046	0.096	0.077	0.065	0.811	0.846	0.778	240	251	245
Little Washita	0.027	0.026	0.042	− 0.057	− 0.032	0.000	0.063	0.041	0.042	0.909	0.910	0.835	259	259	258
South Fork	0.053	0.045	0.061	− 0.084	− 0.087	− 0.074	0.099	0.098	0.095	0.710	0.764	0.668	172	171	171
Little River	0.036	0.029	0.041	0.050	0.078	0.115	0.062	0.083	0.122	0.885	0.872	0.683	193	193	193
Kenaston	0.033	0.027	0.052	− 0.065	− 0.051	− 0.024	0.073	0.057	0.057	0.833	0.828	0.515	186	186	186
Carman	0.087	0.049	0.051	− 0.102	− 0.109	− 0.101	0.134	0.120	0.113	0.406	0.594	0.505	161	162	162
Monte Buey	0.075	0.052	0.046	0.007	− 0.019	− 0.050	0.075	0.056	0.067	0.848	0.874	0.722	107	113	113
REMEDHUS	0.041	0.045	0.055	− 0.029	− 0.018	0.006	0.050	0.048	0.056	0.856	0.857	0.781	168	184	156
Twente	0.068	0.052	0.051	0.006	0.001	− 0.001	0.069	0.052	0.051	0.897	0.903	0.834	272	274	274
HOBE	0.046	0.042	0.069	0.003	− 0.013	− 0.019	0.046	0.044	0.071	0.711	0.844	0.811	106	106	106
Mongolia	0.032	0.038	0.037	− 0.017	− 0.018	− 0.017	0.036	0.042	0.041	0.747	0.700	0.706	110	79	82
Yanco	0.060	0.053	0.052	0.004	0.011	0.013	0.060	0.054	0.054	0.966	0.966	0.940	201	203	199
L2_SM_P_E over a 33 km × 33 km contributing domain	0.047	0.039	0.049	− 0.036	− 0.027	− 0.011	0.070	0.060	0.066	0.772	0.814	0.729			
L2 SMOS averaged over a 33 km × 33 km contributing domain	0.052			− 0.029			0.071			0.721					
L2_SM_P over a 36 km × 36 km contributing domain	0.046	0.039	0.047	− 0.037	− 0.028	− 0.015	0.071	0.061	0.066	0.772	0.795	0.700			
L2 SMOS averaged over a 36 km × 36 km contributing domain	0.053			− 0.028			0.072			0.710					
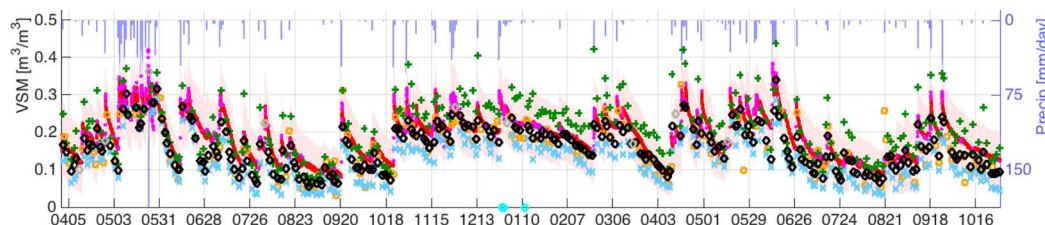
(a) Descending L2_SM_P_E at Little Washita, OK : ubRMSE = 0.022 m³/m³, bias = −0.027 m³/m³, R = 0.920
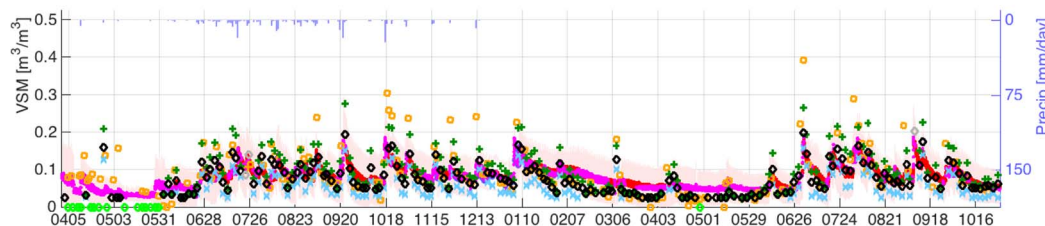
(b) Descending L2_SM_P_E at Walnut Gulch, AZ: ubRMSE = 0.024 m³/m³, bias = 0.011 m³/m³, R = 0.813

Fig. 7. Soil moisture time series at (a) Little Washita, OK; and (b) Walnut Gulch, AZ between April 2015 and October 2016. *In situ* soil moisture data are in magenta, and precipitation data are in blue. Legends: SCA-V (black ◇), SCA-H (blue ×) DCA (green +), and SMOS (orange □), unattempted retrievals (cyan), and failed retrievals (bright green). (For interpretation of the references to colour in this figure legend, the reader is referred to the web version of this article.)

cover a spatial extent similar to the native resolution of the radiometer (Section 2.1). Within this domain, CVS *in situ* data were scaled and aggregated to provide the reference soil moisture for comparison. L2_SM_P_E soil moisture estimates from 6:00 am descending and 6:00 pm ascending overpasses were then extracted to match up in space and time with the corresponding CVS *in situ* data. Table 3 lists the CVSs used in the assessment, along with their geographical locations, climate regimes, and land cover types.

Tables 4 and 5 summarize the performance metrics that characterize the retrieval performance of the 6:00 am descending and 6:00 pm ascending L2_SM_P_E soil moisture estimates at CVSs for the baseline and two other candidate soil moisture retrieval algorithms (SCA-H: Single Channel Algorithm using the H-polarized T_B channel and DCA: Dual Channel Algorithm) (O'Neill et al., 2015). Compared with the other two candidate algorithms, the SCA-V baseline algorithm was able to deliver the best overall retrieval performance, achieving an average ubRMSE of 0.038 m³/m³ (6:00 am descending) and 0.039 m³/m³ (6:00 pm ascending) as well as correlation of 0.819 (6:00 am descending) and

Table 6
Sparse networks used in L2_SM_P_E assessment.

Sparse network	Region
NOAA Climate Reference Network (CRN)	USA
USDA NRCS Soil Climate Analysis Network (SCAN)	USA
GPS	Western USA
COSMOS	Mostly USA
SMOSMania	Southern France
Pampas	Argentina
Oklahoma Mesonet	Oklahoma, USA
MAHASRI	Mongolia

0.814 (6:00 pm ascending). In addition, the 6:00 am estimates were shown to be in closer agreement with the CVS *in situ* soil moisture observations than the 6:00 pm estimates. This asymmetry in performance is particularly noticeable from the bias metric: $-0.015 \ \mathrm{m^3/m^3}$ (6:00 am descending) *vs.* $-0.027 \ \mathrm{m^3/m^3}$ (6:00 pm ascending). The overall dry bias is likely due to the inadequate depth correction for the GMAO ancillary surface temperatures (Table 2) used to account for the difference between the model soil depth and the actual physical sensing soil depth at L-band frequency, although other algorithm assumptions which are more likely to be true at 6:00 am than at 6:00 pm could also contribute to the overall asymmetry in performance. Further refinements in the correction procedure for the effective soil temperature described in (Chan et al., 2016; Choudhury et al., 1982) are expected to improve the observed biases and reduce the performance gap between the 6:00 am and 6:00 pm soil moisture estimates in future updates of the product. Both L2_SM_P_E and L2_SM_P displayed similar retrieval performance when assessed at effectively the same spatial scale.

As an alternate way to present a subset of the tabulated data in Table 4, Fig. 7 shows the time series of L2_SM_P_E at two sample CVSs with low-to-moderate amounts of vegetation. In both sites the soil moisture estimates of L2_SM_P_E tracked the observed dry-down soil moisture trends very well.

3.2. Sparse networks

The sparse networks represent another valuable *in situ* data source contributing to SMAP soil moisture assessment. The defining feature of these networks is that their measurement density is low, usually resulting in (at most) one point within a SMAP radiometer footprint. Although the resulting data alone cannot always provide a representative spatial average of soil moisture at the spatial scale of L2_SM_P_E (Section 2.1) the way the CVS *in situ* data do, they often cover a much larger spatial extent and land cover diversity with very predictable data latency.

Table 6 lists the set of sparse networks used in this assessment study. Compared with (Chan et al., 2016), two additional sparse networks (the Oklahoma Mesonet and the MAHASRI network) were available. The additional data should improve the statistical representativeness of the assessment. Tables 7 and 8 summarize the retrieval performance of the 6:00 am descending and 6:00 pm ascending L2_SM_P_E between April 2015 and October 2016 for the baseline and the other two candidate soil moisture retrieval algorithms. In addition to L2_SM_P_E, the retrieval performance of L2_SM_P and SMOS soil moisture estimates was also provided for comparison. Metrics over land cover classes not represented by any of the sparse networks in Table 6 were not available and hence not reported.

According to Tables 7 and 8, the agreement between L2_SM_P_E and sparse network *in situ* data was not as good as that reported in Tables 4 and 5 with CVS *in situ* data. This is expected because with sparse network *in situ* data there is an additional uncertainty when comparing a footprint-scale soil moisture estimate by the satellite with *in situ* data that are available at only one sensor location within the networks. Overall the performance metrics in Tables 7 and 8 displayed the same trends observed in Tables 4 and 5 with CVS *in situ* data. For example, the SCA-V baseline soil moisture retrieval algorithm was shown to deliver the best overall performance when compared with the other two candidate algorithms. In addition, the 6:00 am descending L2_SM_P_E was shown to be in better agreement with the sparse network *in situ* data than the 6:00 pm ascending L2_SM_P_E – a trend also observed in the previous assessment with CVS *in situ* data. This independent convergence of metric patterns in both CVS and sparse network assessments provides additional confidence in the statistical consistency between these two validation methodologies that differ greatly in the spatial scales that they represent.

4. Conclusion

Following SMOS and Aquarius, SMAP became the third mission in less than a decade utilizing an L-band radiometer to estimate soil moisture from space. The sophisticated RFI mitigation hardware onboard the observatory has enabled acquisition of T_B observations that are relatively well filtered against interferences.

The application of the Backus-Gilbert interpolation technique results in a more optimal capture of spatial information when the original SMAP Level 1B observations are represented on a grid. The resulting gridded T_B data – the SMAP Level 1C Enhanced Brightness Temperature Product (L1C_TB_E) serves as the primary input to the SMAP Level 2 Enhanced Passive Soil Moisture Product (L2_SM_P_E), resulting in soil moisture estimates posted on a 9 km grid.

Based on comparison with *in situ* soil moisture observations from

Table 7
Comparison between the 6:00 am descending L2_SM_P_E and *in situ* soil moisture observations over sparse networks between April 2015 and October 2016.

IGBP Land Cover Class	ubRMSE ($\mathrm{m^3/m^3}$)				Bias ($\mathrm{m^3/m^3}$)				RMSE ($\mathrm{m^3/m^3}$)				Correlation (R)				N
	SCA-H	SCA-V	DCA	SMOS	SCA-H	SCA-V	DCA	SMOS	SCA-H	SCA-V	DCA	SMOS	SCA-H	SCA-V	DCA	SMOS	
Evergreen Needleleaf Forest	0.040	0.039	0.052	0.062	−0.033	0.033	0.166	−0.127	0.052	0.051	0.174	0.141	0.498	0.530	0.515	0.430	1
Mixed Forest	0.059	0.060	0.068	0.055	−0.037	−0.003	0.045	−0.054	0.070	0.060	0.081	0.077	0.609	0.591	0.541	0.752	1
Open Shrublands	0.038	0.039	0.050	0.056	−0.041	−0.008	0.032	−0.010	0.063	0.055	0.075	0.068	0.516	0.523	0.513	0.460	38
Woody Savannas	0.054	0.049	0.061	0.081	−0.017	0.021	0.078	−0.063	0.088	0.080	0.112	0.134	0.709	0.717	0.596	0.541	16
Savannas	0.032	0.032	0.040	0.044	−0.043	−0.026	−0.016	−0.031	0.063	0.055	0.056	0.059	0.877	0.875	0.869	0.866	3
Grasslands	0.051	0.051	0.059	0.062	−0.076	−0.042	0.003	−0.049	0.098	0.079	0.080	0.091	0.667	0.675	0.637	0.596	224
Croplands	0.077	0.066	0.071	0.078	−0.047	−0.033	−0.009	−0.050	0.117	0.101	0.097	0.117	0.569	0.602	0.541	0.553	54
Cropland/Natural Vegetation Mosaic	0.063	0.056	0.066	0.079	−0.044	−0.015	0.033	−0.124	0.095	0.084	0.101	0.176	0.722	0.761	0.643	0.536	20
Barren or Sparsely Vegetated	0.018	0.021	0.030	0.032	−0.015	0.006	0.035	0.002	0.034	0.033	0.051	0.040	0.648	0.596	0.522	0.620	6
L2_SM_P_E averaged over IGBP classes	0.054	0.051	0.060	0.065	−0.062	−0.032	0.010	−0.049	0.095	0.079	0.084	0.098	0.642	0.654	0.608	0.572	363
L2_SM_P averaged over IGBP classes	0.053	0.050	0.057	0.066	−0.061	−0.031	0.010	−0.049	0.093	0.077	0.081	0.099	0.643	0.663	0.633	0.576	393

Table 8
Comparison between the 6:00 pm ascending L2_SM_P_E and *in situ* soil moisture observations over sparse networks between April 2015 and October 2016.

	ubRMSE (m³/m³)				Bias (m³/m³)				RMSE (m³/m³)				Correlation (*R*)				*N*
	SCA-H	SCA-V	DCA	SMOS	SCA-H	SCA-V	DCA	SMOS	SCA-H	SCA-V	DCA	SMOS	SCA-H	SCA-V	DCA	SMOS	
Evergreen Needleleaf Forest	0.047	0.046	0.067	0.050	−0.057	0.006	0.115	−0.095	0.074	0.047	0.133	0.107	0.442	0.461	0.429	0.585	1
Mixed Forest	0.057	0.053	0.051	0.056	−0.040	−0.011	0.029	−0.047	0.070	0.054	0.059	0.073	0.687	0.740	0.771	0.753	1
Open Shrublands	0.040	0.042	0.053	0.057	−0.051	−0.022	0.009	−0.005	0.070	0.058	0.067	0.071	0.485	0.468	0.441	0.421	39
Woody Savannas	0.051	0.047	0.058	0.080	−0.012	0.015	0.053	−0.045	0.086	0.079	0.098	0.114	0.745	0.750	0.625	0.584	16
Savannas	0.033	0.035	0.040	0.047	−0.043	−0.034	−0.029	−0.023	0.063	0.058	0.058	0.073	0.890	0.871	0.861	0.841	3
Grasslands	0.051	0.051	0.059	0.062	−0.079	−0.053	−0.020	−0.043	0.101	0.085	0.082	0.088	0.663	0.667	0.632	0.609	224
Croplands	0.075	0.065	0.070	0.076	−0.037	−0.037	−0.030	−0.047	0.117	0.103	0.100	0.111	0.579	0.610	0.560	0.547	54
Cropland/Natural Vegetation Mosaic	0.061	0.055	0.065	0.079	−0.033	−0.017	0.009	−0.112	0.089	0.083	0.093	0.160	0.723	0.761	0.659	0.544	20
Barren or Sparsely Vegetated	0.019	0.022	0.031	0.036	−0.022	−0.005	0.018	0.004	0.038	0.035	0.045	0.045	0.577	0.516	0.443	0.453	6
L2_SM_P_E averaged over IGBP classes	0.053	0.051	0.059	0.065	−0.063	−0.041	−0.012	−0.043	0.097	0.083	0.084	0.094	0.639	0.645	0.601	0.575	364
L2_SM_P averaged over IGBP classes	0.053	0.051	0.059	0.065	−0.063	−0.043	−0.016	−0.043	0.097	0.083	0.084	0.095	0.618	0.629	0.595	0.578	394

CVSs, it was found that the SCA-V baseline soil moisture algorithm resulted in the best retrieval performance compared with the other two candidate algorithms considered in this assessment. The ubRMSE, bias, and correlation of the 6:00 am descending baseline soil moisture estimates were found to be 0.038 m³/m³, −0.015 m³/m³, and 0.819, respectively. The metrics for the 6:00 pm ascending baseline soil moisture estimates were slightly worse in comparison but nonetheless similar overall. It is expected that further refinements in the correction procedure for the effective soil temperature will improve the observed biases and reduce the performance gap between the 6:00 am and 6:00 pm soil moisture estimates in future updates of the product.

Acknowledgment

References

SMAP Algorithm Development Team, SMAP Science Team, 2015. SMAP Ancillary Data Report on Surface Temperature. Jet Propulsion Laboratory, California Institute of Technology, Pasadena, CA (JPL D-53064). http://smap.jpl.nasa.gov/system/internal_resources/details/original/293_051_surf_temp_150304.pdf (accessed: February 10, 2017).
Bradley, J.P., Long, D.G., 2014. Estimation of the OSCAT spatial response function using island targets. IEEE Trans. Geosci. Remote Sens. 52 (4), 1924–1934.
Brodzik, M.J., Billingsley, B., Haran, T., Raup, B., Savoie, M.H., 2012. EASE-grid 2.0: incremental but significant improvements for Earth-gridded data sets. ISPRS Int. J. Geo-Inf. 1 (1), 32–45.
Brodzik, M.J., Billingsley, B., Haran, T., Raup, B., Savoie, M.H., 2014. Correction: Brodzik, M.J. et al. EASE-grid 2.0: incremental but significant improvements for Earth-gridded data sets. ISPRS Int. J. Geo-Inf. 1 (1), 32–45 (2012, ISPRS International Journal of Geo-Information, 3(3), pp. 1154–1156).
Chan, S.K., 2013. SMAP Ancillary Data Report on Static Water Fraction. Jet Propulsion Laboratory, California Institute of Technology, Pasadena, CA (JPL D-53059). http://smap.jpl.nasa.gov/system/internal_resources/details/original/287_045_water_frac.pdf (accessed: February 10, 2017).
Chan, S.K., 2016. SMAP Enhanced Level 2 Passive Soil Moisture Data Product Specification Document. Jet Propulsion Laboratory, California Institute of Technology, Pasadena, CA (JPL D-56291). http://nsidc.org/sites/nsidc.org/files/files/D56291%20SMAP%20L2_SM_P_E%20PSD%20Version%201.pdf (accessed: February 10, 2017).
Chan, S.K., Dunbar, R.S., 2016. SMAP Enhanced Level 1C Radiometer Data Product Specification Document. Jet Propulsion Laboratory, California Institute of Technology, Pasadena, CA (JPL D-56290). https://nsidc.org/sites/nsidc.org/files/technical-references/D56290%20SMAP%20L1C_TB_E%20PSD%20Version%201.pdf (accessed: February 10, 2017).

Chan, S.K., Bindlish, R., Hunt, R., Jackson, T., Kimball, J., 2013. SMAP Ancillary Data Report on Vegetation Water Content. Jet Propulsion Laboratory, California Institute of Technology, Pasadena, CA (JPL D-53061). http://smap.jpl.nasa.gov/system/internal_resources/details/original/289_047_veg_water.pdf (accessed: February 10, 2017).
Chan, S.K., Njoku, E., Colliander, A., 2014. SMAP Algorithm Theoretical Basis Document: Level 1C Radiometer Data Product. Jet Propulsion Laboratory, California Institute of Technology, Pasadena, CA (JPL D-53053). http://smap.jpl.nasa.gov/system/internal_resources/details/original/279_L1C_TB_ATBD_RevA_web.pdf (accessed: February 10, 2017).
[dataset] S.K. Chan, S.K. E. Njoku, E. A. Colliander, A.2015. SMAP L1C Radiometer Half-orbit 36 km EASE-grid Brightness Temperatures, Version 3. NASA National Snow and Ice Data Center Distributed Active Archive Center, Boulder, CO.
Chan, S.K., Bindlish, R., O'Neill, P., Njoku, E., Jackson, T., Colliander, A., Chen, F., Mariko, M., Dunbar, S., Piepmeier, J., Yueh, S., Entekhabi, D., Cosh, M.H., Caldwell, T., Walker, J., Wu, X., Berg, A., Rowlandson, T., Pacheco, A., McNairn, H., Thibeault, M., Martinez-Fernandez, J., Gonzalez-Zamora, A., Seyfried, M., Bosch, D., Starks, P., Goodrich, D., Prueger, J., Palecki, M., Small, E.E., Zreda, M., Calvet, J., Crow, W.T., Kerr, Y., 2016. Assessment of the SMAP passive soil moisture product. IEEE Trans. Geosci. Remote Sens. 54 (8), 4994–5007.
Chaubell, J., 2016. SMAP Algorithm Theoretical Basis Document: Enhanced L1B Radiometer Brightness Temperature Product. Jet Propulsion Laboratory, California Institute of Technology, Pasadena, CA (JPL D-56287). https://nsidc.org/files/technical-references/SMAP_L1B_TB_E_Product_ATBD_D-56287.pdf (accessed: February 10, 2017).
[dataset] J. Chaubell, J. S.K. Chan, S.K. R. Dunbar, R. J. Peng, R. J. S. Yueh, S.2016. SMAP Enhanced L1C Radiometer Half-orbit 9 km EASE-Grid Brightness Temperatures, Version 1. NASA National Snow and Ice Data Center Distributed Active Archive Center, Boulder, CO.
Chen, F., Crow, W.T., Colliander, A., Cosh, M.H., Jackson, T., Bindlish, R., Reichle, R., Chan, S.K., Bosch, D., Starks, P., Goodrich, D., Seyfried, M., 2017. Application of triple collocation in ground-based validation of soil moisture active/passive (SMAP) level 2 data products. IEEE J. Sel. Top. Appl. Earth Obs. Remote Sens. 10 (2), 489–502.
Choudhury, B.J., Schmugge, T.J., Mo, T., 1982. A parameterization of effective soil temperature for microwave emission. J. Geophys. Res. 87, 1301–1304.
Colliander, A., Jackson, T., Bindlish, R., Chan, S.K., Kim, S., Cosh, M.H., Dunbar, R., Dang, L., Pashaian, L., Asanuma, J., Aida, K., Berg, A., Rowlandson, T., Bosch, D., Caldwell, T., Caylor, K., Goodrich, D., al Jassar, H., Lopez-Baeza, E., Martinez-Fernandez, J., Gonzalez-Zamora, Á., Livingston, S., McNairn, H., Pacheco, A., Moghaddam, M., Montzka, C., Notarnicola, C., Niedrist, G., Pellarin, T., Prueger, J., Pulliainen, J., Rautiainen, K., Ramos, J., Seyfried, M., Starks, P., Su, Z., Zeng, Y., van der Velde, R., Thibeault, M., Dorigo, W., Vreugdenhil, M., Walker, J.P., Wu, X., Monerris, A., O'Neill, P.E., Entekhabi, D., Njoku, E.G., Yueh, S., 2017. Validation of SMAP surface soil moisture products with core validation sites. Remote Sens. Environ. 191, 215–231.
Das, N., 2013a. SMAP Ancillary Data Report on Urban Area. Jet Propulsion Laboratory, California Institute of Technology, Pasadena, CA (JPL D-53060). http://smap.jpl.nasa.gov/system/internal_resources/details/original/288_046_urban_area_v1.1.pdf (accessed: February 10, 2017).
Das, N., 2013b. SMAP Ancillary Data Report on Soil Attributes. Jet Propulsion Laboratory, California Institute of Technology, Pasadena, CA (JPL D-53058). http://smap.jpl.nasa.gov/system/internal_resources/details/original/286_044_soil_attrib.pdf (accessed: February 10, 2017).
Dunbar, R.S., 2013. SMAP Ancillary Data Report on Precipitation, Jet Propulsion Laboratory. California Institute of Technology, Pasadena, CA(JPL D-53063). http://smap.jpl.nasa.gov/system/internal_resources/details/original/291_049_precip.pdf (accessed: February 10, 2017).
Entekhabi, D., Reichle, R., Koster, R., Crow, W.T., 2010. Performance metrics for soil moisture retrievals and application requirements. J. Hydrometeorol. 11, 832–840.
Entekhabi, D., Yueh, S., O'Neill, P., Kellogg, K., 2014. SMAP Handbook – Soil Moisture

Active Passive: Mapping Soil Moisture and Freeze/thaw From Space. SMAP Project, Jet Propulsion Laboratory, Pasadena, CA.

Jackson, T., O'Neill, P., Chan, S.K., Bindlish, R., Colliander, A., Chen, F., Dunbar, S., Piepmeier, J., Cosh, M.H., Caldwell, T., Walker, J., Wu, X., Berg, A., Rowlandson, T., Pacheco, A., McNairn, H., Thibeault, M., Martínez-FernÁndez, J., GonzÁlez-Zamora, Á., Lopez-Baeza, E., Uldall, F., Seyfried, M., Bosch, D., Starks, P., Holifield Collins, C., Prueger, J., Su, Z., van der Velde, R., Asanuma, J., Palecki, M., Small, E.E., Zreda, M., Calvet, J., Crow, W.T., Kerr, Y., Yueh, S., Entekhabi, D., 2016. Calibration and Validation for the L2/3_SM_P Version 4 and L2/3_SM_P_E Version 1 Data Products. Jet Propulsion Laboratory, California Institute of Technology, Pasadena CA (JPL D-56297). http://nsidc.org/sites/nsidc.org/files/files/D56297%20SMAP%20L2_SM_P_E%20Assessment%20Report(1).pdf (accessed: February 10, 2017).

Kerr, Y.H., Al-Yaari, A., Rodriguez-Fernandez, N., Parrens, M., Molero, B., Leroux, D., Bircher, S., Mahmoodi, A., Mialon, A., Richaume, P., Delwart, S., Al Bitar, A., Pellarin, T., Bindlish, R., Jackson, T.J., Rüdiger, C., Waldteufel, P., Mecklenburg, S., Wigneron, J.-P., 2016. Overview of SMOS performance in terms of global soil moisture monitoring after six years in operation. Remote Sens. Environ. 180, 40–63.

Kim, S., 2013. SMAP Ancillary Data Report on Landcover Classification. Vols. JPL D-53057 Jet Propulsion Laboratory, California Institute of Technology, Pasadena, CA. http://smap.jpl.nasa.gov/system/internal_resources/details/original/284_042_landcover.pdf (accessed: February 10, 2017).

Kim, E., Molotch, N., 2011. SMAP Ancillary Data Report on Snow. NASA Goddard Space Flight Center, Greenbelt, MD (GSFC-SMAP-007).

Koster, R., Brocca, L., Crow, W.T., Burgin, M., De Lannoy, G., 2016. Precipitation estimation using L-band and C-band soil moisture retrievals. Water Resour. Res. 52 (9), 7213–7225.

Mohammed, P.N., Aksoy, M., Piepmeier, J.R., Johnson, J.T., Bringer, A., 2016. SMAP L-Band Microwave Radiometer: RFI Mitigation Prelaunch Analysis and First Year On-Orbit Observations. IEEE Trans. Geosci. Remote Sens. 54 (10), 6035–6047.

O'Neill, P.E., Njoku, E.G., Jackson, T., Chan, S.K., Bindlish, R., 2015. SMAP Algorithm Theoretical Basis Document: Level 2 & 3 Soil Moisture (Passive) Data Products. Jet Propulsion Laboratory, California Institute of Technology, Pasadena, CA (JPL D-66480). http://smap.jpl.nasa.gov/system/internal_resources/details/original/316_L2_SM_P_ATBD_v7_Sep2015.pdf (accessed: February 10, 2017).

[dataset] P.E. O'Neill, P.E. S.K. Chan, S.K. E.G. Njoku, E.G. T. Jackson, T. R. Bindlish, R.2016. SMAP Enhanced L2 Radiometer Half-orbit 9 km EASE-grid Soil Moisture, Version 1. NASA National Snow and Ice Data Center Distributed Active Archive Center, Boulder, CO.

[dataset] J.R. Piepmeier, J.R. P. Mohammed, P. J. Peng, J. E.J. Kim, E.J. G. De Amici, G. C. Ruf, C.2015a. SMAP L1B Radiometer Half-orbit Time-ordered Brightness Temperatures, Version 3. NASA National Snow and Ice Data Center Distributed Active Archive Center, Boulder, CO.

Piepmeier, J.R., et al., 2015b. SMAP Algorithm Theoretical Basis Document: L1B Radiometer Product. NASA Goddard Space Flight Center, Greenbelt, MD (GSFC-SMAP-006). http://smap.jpl.nasa.gov/system/internal_resources/details/original/278_L1B_TB_RevA_web.pdf (accessed: February 10, 2017).

Piepmeier, J.R., Chan, S.K., Chaubell, J., Peng, J., Bindlish, R., Bringer, A., Colliander, A., De Amici, G., Dinnat, E.P., Hudson, D., Jackson, T., Johnson, J., Le Vine, D., Meissner, T., Misra, S., Mohammed, P., Entekhabi, D., Yueh, S., 2016. SMAP Radiometer Brightness Temperature Calibration for the L1B_TB (Version 3), L1C_TB (Version 3), and L1C_TB_E (Version 1) Data Products. Jet Propulsion Laboratory, California Institute of Technology, Pasadena, CA (JPL D-56295). https://nsidc.org/sites/nsidc.org/files/files/D56295%20SMAP%20L1C_TB_E%20Assessment%20Report.pdf (accessed: February 10, 2017).

Podest, E., Crow, W.T., 2013. SMAP Ancillary Data Report on Digital Elevation Model. Jet Propulsion Laboratory, California Institute of Technology, Pasadena, CA (JPL D-53056). http://smap.jpl.nasa.gov/system/internal_resources/details/original/285_043_dig_elev_mod.pdf (accessed: February 10, 2017).

Poe, G., 1990. Optimum interpolation of imaging microwave radiometer data. IEEE Trans. Geosci. Remote Sens. 28 (5), 800–810.

Smith, A.B., Walker, J.P., Western, A.W., Young, R.I., Ellett, K.M., Pipunic, R.C., Grayson, R.B., Siriwidena, L., Chiew, F.H.S., Richter, H., 2012. The Murrumbidgee soil moisture monitoring network data set. Water Resour. Res. 48 (7), W07701.

Stogryn, A., 1978. Estimates of brightness temperatures from scanning radiometer data. IEEE Trans. Antennas Propag. AP-26, 720–726.

Torres, R., Snoeij, P., Geudtner, D., Bibby, D., Davidson, M., Attema, E., Potin, P., Rommen, B., Floury, N., Brown, M., Navas-Traver, I., Deghaye, P., Duesmann, B., Rosich, B., Miranda, N., Bruno, C., L'Abbate, M., Croci, R., Pietropaolo, A., Huchler, M., Rostan, F., 2012. GMES Sentinel-1 mission. Special Issue of Journal of Remote Sensing of Environment on the Sentinel Missions - New Opportunities for Science 120, 9–24.

Yee, M.S., Walker, J.P., Monerris, A., Rüdiger, C., Jackson, T.J., 2016. On the identification of representative in-situ soil moisture monitoring stations for the validation of SMAP soil moisture products in Australia. J. Hydrol. 537, 367–381.

Yueh, S.H., Fore, A., Tang, W., Hayashi, A., Stiles, B., Reul, N., Weng, Y., Zhang, F., 2016. SMAP L-band passive microwave observations of ocean surface wind during severe storms. IEEE Trans. Geosci. Remote Sens. 54 (12), 7339–7350.